Iranian Journal of Science and Technology, Transactions of Civil Engineering
https://doi.org/10.1007/s40996-026-02161-9

RESEARCH PAPER

Comparative Experimental Study for Flexural Performance of Engineered Cementitious Reinforced Concrete Beams

Mohamed Said[1] · Maher A. Adam[2] · Mahmoud Abbass[2] · Ahmed Salah[2]

Received: 28 September 2025 / Accepted: 11 April 2026

Abstract

This study investigates the flexural behavior of high-performance reinforced concrete (HPRC) beams reinforced with glass fiber-reinforced polymer (GFRP) and high-tensile steel (HTS) longitudinal bars, and containing short innovation fibers. Carbon (CA) and polyvinyl alcohol (PVA) fibers are incorporated to enhance the strength and ductility of non-fiber-reinforced concrete beams. Seven supported HPRC beams were constructed and tested to investigate the effects of fiber volume fraction (*Vf*), reinforcement ratio (ρt) of GFRP and HTS bars, and fiber type on flexural performance. CA fibers increase the yield and ultimate flexural load by 51% and 32%, respectively. Hybrid (CA-PVA) fibers improved *Py* and *Pu* by 36% and 24%.%. Furthermore, flexural toughness (I) and flexural strength increased by 68% and 10%, respectively, with the inclusion of PVA fibers at a volume fraction *(Vf) of* 1.2%. The hybrid (CA-PVA) fiber increased the yield and post-cracking stiffness by 18% and 21%, respectively. GFRP bars with $\rho f = 1.45\%$ improved the ultimate flexural load by 21%. ANSYS 15.0, nonlinear finite element analysis (NFEA) software, is used to validate the experimental work results. The NFEA results, which relate to the correlation between load capacity and deflection, as well as the observed crack patterns, closely matched the experimental data. An improved empirical formula based on ACI 318−19 (Building code requirements for structural concrete, American Concrete Institute; Farmington Hills 2019) was proposed to determine the nominal flexural strength of High-Performance RC beams. The nominal values obtained from the improved empirical formula correlate well with the experimental results.

Keywords Flexural strength · Experimental · Carbon fibers · Hybrid fibers · PVA fibers · GFRP · Finite element · Numerical analysis · NFEA

Abbreviations

ρs	Longitudinal steel reinforcement ratio
ρf	Longitudinal GFRP bars ratio
ρt	Total reinforcement ratio
b	Width of HPRC beam
d	The depth of HPRC beam
t	Thickness HPRC beam
l_f	Length of short fibers
ϕf	Short fiber diameter
fc(exp.)'	The concrete cylinder experimental compressive strength
Pcr, exp.	Experimental cracking load
$\delta cr, exp.$	Experimental deflection at first cracking
Pu, exp.	Experimental ultimate flexural load
Pu, NA.	Numerical ultimate load
$\delta u, exp.$	Experimental ultimate deflection
$\delta u, NA.$	Numerical ultimate deflection
Py, exp.	Experimental yield flexural load

✉ Mahmoud Abbass
mahmoud.abbas@feng.bu.edu.eg

Mohamed Said
mohamed.abdelghaffar@feng.bu.edu.eg;
mohamed.said@eng.bnu.edu.eg

Maher A. Adam
maher.adam@feng.bu.edu.eg

Ahmed Salah
ahmed.salaheldin@feng.bu.edu.eg

[1] Dean Faculty of Engineering (Shoubra), Benha University, Cairo, Egypt

[2] Faculty of Engineering (Shoubra), Benha University, Cairo, Egypt

Published online: 08 May 2026

$\delta y, exp.$	Experimental yield deflection
$Py, NA.$	Numerical yielding flexural load
$\delta y, NA.$	Numerical yielding deflection
$Ka, exp.$	Experimental yield stiffness
$Kp, exp.$	Experimental post-cracking stiffness
$I, exp.$	Experimental flexural toughness
DF, exp	Experimental ductility factor
εy	experimental yield strain
εu	experimental ultimate strain
μs	experimental strain ductility
Ts	tension force in steel bars
As	area of steel bars
T_{GFRP}	tension force in GFRP bars
A_{GFRP}	area of GFRP bars
V_f	volume of fiber
$\sigma fiber$	the fibrous- concrete tensile strength
T_{fiber}	tension force in short fibers
e	distance from extreme tension fiber to the neutral axis of the tensile stress block
Fbe	Fibers bond efficiency factor
$Mexp.$	experimental bending moment
$Mn.$	Nominal bending moment

1 Introduction

Concrete structures have become widespread in modern society due to their outstanding compressive strength. However, concrete has low tensile strength, so it is reinforced with steel to ensure adequate tensile capacity. High-tensile steel (HTS) is the most commonly used material for strengthening concrete structures. However, steel is susceptible to corrosion, a drawback that rivals Fiber Reinforcement Polymer (FRP) bars, which are often used as an alternative to HTS bars due to their superior tensile strength and non-corrosive properties (Pawłowski and Szumigała 2015). Moreover, the flexural properties of concrete can also be enhanced beyond its inherent compressive and tensile strength through ductility. The incorporation of various short fibers into concrete mixtures enhances properties and improves performance. By selecting and combining the most appropriate short fibers based on their type or content, the flexural properties of concrete can be positively influenced. In this research, CA, PVA fibers, and GFRP bars will be used to enhance the properties of RC beams.

Steel reinforcement bars are particularly vulnerable to corrosion, a leading cause of reduced service life in reinforced concrete structures. To satisfy ultimate limit-state and durability requirements, corrosion-resistant reinforcement bars may need to be replaced or coated with corrosion-resistant materials. Fiber-reinforced polymer (FRP) bars, typically composed of carbon, glass, or aramid fibers, offer high specific strength and inherent corrosion resistance, making them suitable replacements for steel reinforcement. Several studies have investigated the performance of concrete beams reinforced with FRP bars (Adam et al. 2015, Dong et al. 2019, Pawłowski and Szumigała 2015, Tomlinson 2015, Douglas 2012, Soric et al. 2010). Under tensile loading, FRP bars exhibit a linearly elastic stress–strain regime until failure, characterized by a lower elastic modulus and a lack of ductility relative to steel (Raffaello et al.). As a result, FRP-reinforced beams are likely to exhibit larger deflections, larger crack widths, and brittle failure modes. Nevertheless, testing has shown that failure primarily occurs by compression, which has led to the recommendation that FRP reinforcement should not be used in moment-resisting frames (Tu et al. 2009, Habeeb and Ashour 2008, Pecce et al. 2000, Said et al. 2016). A significant amount of research has been done to develop and improve fiber-reinforcing materials for concrete structures. It has been demonstrated that incorporating short steel fibers significantly enhances the structural strength of concrete members (Liew and Akbar 2020, Romualdi and Mandel 1964, Romualdi and Batson 1963). In addition, incorporating materials such as glass, carbon, and synthetic fibers enhances various properties of concrete (Liu et al. 2020, Charron et al. 2020, Rafid 2019). Among these materials, carbon fibers feature high tensile strength and modulus, low density, and excellent durability.

Moreover, within the cement matrix, the incorporation of carbon fibers has been reported to enhance the structural properties of concrete beams. By reinforcing concrete beams with carbon fibers, the flexural strength and toughness are significantly improved (Gao et al. 2018). The incorporation of two or more types of short fibers into the concrete mix improves all performance aspects of the concrete structure. Hybrid fibers are introduced into concrete beams to improve their multiple properties (Shanour et al. 2018, Asok and George 2016, Said et al. 2023). Shanour and colleagues (2018) conducted 12 experimental trials on reinforced concrete beams reinforced with engineered cementitious composite (ECC). In the study, the reinforcement ratio (ρs) of the steel was changed systematically, while also altering the height of the ECC layer at the cross-section of the beam, as well as the inclusion of fiber type (polyvinyl alcohol (PVA) or polypropylene (PP)), with fiber dosage as a percentage of the mix. Each specimen beam was evaluated for mid-span deflection, crack pattern, and ultimate load capacity. Specimens reinforced with PVA fibers showed an advantage over specimens reinforced with PP fibers. George (2016) studied the effects of hybrid combinations of steel and polypropylene (PP) fibers in RC beams, with ratios of 1% for steel and 0.35% for short (PP) fibers. Hybrid fibers, therefore, produced a better flexural tensile strength than non-fibrous concrete. Said et al. (2023) analyzed how the hybrid fibers

affected the torsional strength of RC beams. The research involved mixing carbon, basalt, and steel fibers into concrete for the tested mixes. In contrast, the others introduce different types of fibers into the mixture by up to 65.2%, whereas the highest ductility increase of 84.8% was achieved with a mix of basalt and steel fibers.

Guo et al. (2021) investigated the impact of both carbon fiber length and dosage on the residual mechanical properties and microstructure of carbon fiber–reinforced concrete (CFRC) subjected to high temperatures. Seven fresh mixes were prepared by mixing carbon fiber with concrete, with variable fiber lengths (up to 10 mm) and fiber contents (up to 1.0 wt%). These mixes were evaluated based on their compressive, splitting, and flexural strengths. Here, the addition of carbon fiber had a slight effect on compressive strength but substantially increased splitting and flexural strengths.

Wang et al. (2021) introduced a new casting method to achieve an even distribution of 20 mm carbon fibers in reinforced concrete beam specimens of varying fiber volume fractions. Based on the mechanical tests, it was concluded that beams with 0.35% fiber content absorbed the most energy. Compared with the 0.35% and 0.40% fiber-content mixtures, the other mixtures exhibited higher tensile and compressive strains. Li et al. (2018) conducted four-point bending tests on 51 specimens of hybrid fibre-reinforced concrete by incorporating monofilament polypropylene fibres with straight, corrugated, or hooked-end steel fibres to assess load–deflection behaviour, crack progression, and toughness. All hybrid configurations yielded synergistic improvements in flexural performance, with specimens containing hooked-end fibers exhibiting the highest strength and toughness.

Smarzewski (2018) examined the hybrid of steel-polypropylene fibers as a strengthening strategy for reinforced high-performance concrete (HPC) beams with and without web openings. In this case, various fiber contents were used to replace conventional stirrups and compressive bars. The experimental results indicated that increasing the fiber dosage significantly improved the shear performance of the beams, as evidenced by larger loads at diagonal cracking and ultimate shear strength.

Saingam et al.(2025) conducted research on the sustainable creation of eco-friendly self-consolidating mortar (SCM), focusing on the use of waste glass as a partial or complete replacement for fine aggregate due to significant environmental issues. The findings revealed that the self-consolidating properties of SCM were maintained, with mini-slump flow values ranging from 233 mm to 263 mm, which are within the EFNARC-recommended limits, even with 100% waste glass replacement and a 15% addition of electronic waste fibers.

Suparp et al. (2023) conduct an experimental and finite element analysis of reinforced concrete beams characterized by solid, hollow, prismatic, or non-prismatic sections. The findings indicate that shear intensity was highest in prismatic-section beams. Rodsen et al. (2023) developed an experimental framework involving seventeen beams to examine the effects of loading type, configuration, and through-bolt anchorage on the performance of LC-GFRP (Low-Cost Glass-Fiber-Reinforced Polymer) confinement. The study revealed that beams reinforced with LC-GFRP wraps and anchors exhibited different outcomes. Specifically, side-bonded configurations experienced debonding and shear failure, whereas U-shaped configurations applied exclusively to the shear span effectively prevented the shear failure.

Joyklad (2024) experimented to fill some gaps in knowledge. They used three wire-mesh sizes: small (Type I), medium (Type II), and large (Type III). They attached ferrocement jackets using chemical or mechanical anchors. They used 6, 12, or 18 anchors to see how the number of anchors affected the results. All slabs exhibited ductile failure, with the primary cracks being flexural in nature. Using wire mesh with mechanical anchors slightly increased peak loads by up to 14.29%. Yooprasertchai et al. (2024) conducted a study aimed at the sustainable and innovative development of concrete utilizing both treated and untreated plastic waste aggregates. It was observed that the compressive strength of E-WAC exhibited a negative linear trend with increasing percentages of Elec-waste aggregates.

The flexural performance of basalt fiber reinforced concrete (BFRC) beams reinforced with steel and BFRP bars has been investigated by Wei et al. (2025) through experimental testing, theoretical analysis, and FEM simulations. The outcome of this study reveals that the moment-deflection response of beams reinforced with BFRP is bilinear due to the linear-elastic properties of the BFRP bars. Greater reinforcement ratios were effective in improving flexural strength for steel- and BFRP-reinforced beams. Wei et al. (2025) evaluated the influence of hybrid fibers on the mechanical strength of high-strength concrete (HSC) as well as the flexural toughness ratio of the beam for twenty-one mix proportions, including conventional HSC, singly doped water-treated steel fiber (WSF)-reinforced HSC, and hybrid fiber combinations. The results show that the addition of hybrid fibers significantly increases compressive strength, splitting tensile strength, and uniaxial tensile strength. More specifically, the WSF-SSF hybrid fiber composition demonstrated the most significant improvement, with the compressive strength rising 21.3–25.7% and the splitting tensile strength 32.8–41.4% over the conventional HSC.

Table 1 Mechanical properties of the reinforcing bars and stirrups

Reinforcement type	Diameter (mm)	Yield Strength (fy) Mpa	Ultimate Strength (fu) Mpa	Young's Modulus (E) Gpa
MS	8	240	350	200
HTS	10 and 12	400	600	200
GFRP	10	-	900	45
GFRP	12	-	850	42.5

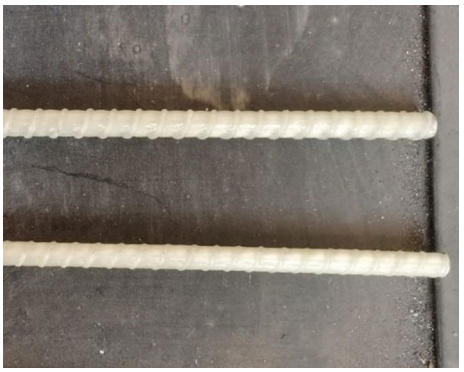

Fig. 1 Ribbed Bars of GFRP with (10 mm and 12 mm)

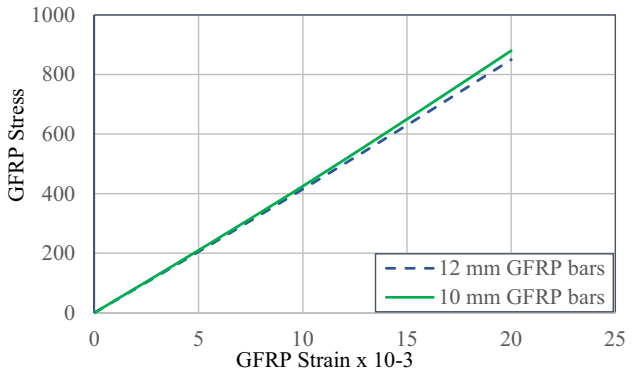

Fig. 2 Stress-Strain Curves for GFRP Bars

2 Research Significant

Extensive research has examined the flexural behavior of reinforced concrete beams with either single-fiber or hybrid fiber reinforcement. Conversely, the use of carbon (CA) fibers and a hybrid of polyvinyl alcohol (PVA) and CA to improve the flexural properties of high-performance RC sections reinforced with GFRPs and high-tensile steel has received limited attention. This research aims to bridge a research gap. It investigates the flexural performance of high-performance RC sections reinforced with different combinations of CA and PVA fibers and GFRP and high-tensile steel. Additionally, the effects of the test variables on the structural response parameters are evaluated.

3 Experimental Test Program

3.1 Materials Properties

3.1.1 High-Tensile Steel and GFRP Bars

The longitudinal reinforcement comprises high-tensile steel with a yield strength of 400 MPa. The stirrups are executed from mild steel bars with an 8 mm diameter, and the Young's modulus for all steel bars in this study is approximately 200 GPa, as indicated in Table 1. The longitudinal bottom reinforcement bars in HTS are selected with diameters of 10 and 12 mm, with an ultimate tensile strength of 600 MPa. The GFRP bars were produced using glass roving and resin. A specialized workshop fabricated longitudinal bars with diameters of 12 mm and 10 mm, as depicted in Fig. 1. The GFRP ultimate strengths of 10 and 12 mm bars reach 900 and 850 MPa, respectively. The Young's modulus of the GFRP bars for 10 mm and 12 mm is 45 and 42.5 GPa, respectively. Experimental tests were conducted on these GFRP bar specimens to evaluate their mechanical properties. Figure 2 illustrates the average tensile strength for each GFRP bar with diameters of 10 mm and 12 mm, respectively.

3.1.2 Properties of Short Fibers

The study examines the experimental results from seven high-performance reinforced concrete (RC) beams incorporating one or more types of short fibers. Carbon (CA) fibers were chosen due to their high modulus of elasticity and tensile strength. Polyvinyl Alcohol (PVA) fibers were selected for their high elongation and ductility. The lengths of monofilament CA and PVA fibers are 10 mm and 8 mm, respectively. The fiber's diameters were measured as 0.01 and 0.015 for CA and PVA, respectively. CA fibers have high tensile strength, reaching 3600 MPa, compared with PVA fibers, which have a tensile strength of 1620 MPa. On the other hand, PVA fibers have a higher elongation value compared with CA fibers; PVA fibers have 5.2% and CA fibers have 3.9%. Young's Modulus is highly indicative of flexural performance; therefore, CA fibers are chosen with a modulus of 160 GPa, and PVA fibers are measured at 34 GPa. The actual lengths and diameters of the fibers are summarized in Table 2, and the shapes of the fibers are indicated in Fig. 3.

Table 2 Carbon and polyvinyl alcohol (PVA) fibers properties

Type	Length of fiber (*lf*) (mm)	Shape	Diameter of fiber (ϕf) (mm)	Tensile Strength (MPa)	Young Modulus (GPa)	Density (ρ) (g/cm^3)	Elongation (%)
Carbon	10	Monofilament	0.01	3600	160	1.76	3.9
PVA	8	Monofilament	0.015	1620	34	1.3	5.2

Fig. 3 CA and PVA Fibers Shape

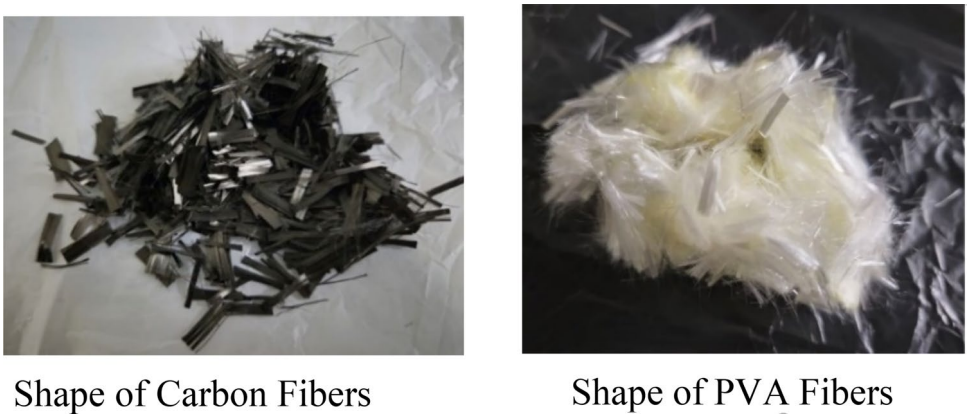

Table 3 Compressive and Splitting Tensile Strength of Concrete Mixtures

Mix No.	The Contents of 1 m^3 of Concrete (kg)									
	Cement	Sand	Coarse aggregate	Water	Carbon Fiber (Vf %)	PVA Fiber (Vf %)	HRWR	Averagen Cylindrical Compressive Strength (MPa)	Average Splitting Tensile Strength (MPa)	Slump Test (mm)
Mix 1	475	620	1180	200	0	0	10	44	3.64	150
Mix 2	475	620	1180	200	1.2	0	18	50.3	4.85	129
Mix 3	475	620	1180	200	0.6	0.6	15	48.4	4.26	132
Mix 4	475	620	1180	200	0	1.2	16	46.5	3.94	144

Table 4 Details of the Tested Specimens

Group	Specimens	Bottom RF	Top RFT	*Vf* (Carbon)%	*Vf* (PVA)%	Bottom RFT %			b (mm)	t (mm)	Stirrups/m
						ρ_s	ρ_f	ρ_t			
A	S1	2Φ12+2Φ10	2Φ8	0	0	1.45%	-	1.45%	120	250	10Φ8/m
	S2	2Φ12+2Φ10	2Φ8	1.2	0	1.45%	-	1.45%	120	250	10Φ8/m
B	S3	2G12+2G10	2Φ8	0	0	-	1.45%	1.45%	120	250	10Φ8/m
	S4	2G12+2G10	2Φ8	0.6	0.6	-	1.45%	1.45%	120	250	10Φ8/m
	S5	2G12+2G10	2Φ8	0	1.2	-	1.45%	1.45%	120	250	10Φ8/m
	S6	2G12+2G10	2Φ8	1.2	0	-	1.45%	1.45%	120	250	10Φ8/m
C	S2	2Φ12+2Φ10	2Φ8	1.2	0	1.45%	-	1.45%	120	250	10Φ8/m
	S7	2G12+2Φ10	2Φ8	1.2	0	0.59%	0.86%	1.45%	120	250	10Φ8/m
	S6	2G12+2G10	2Φ8	1.2	0	-	1.45%	1.45%	120	250	10Φ8/m

3.1.3 Concrete Mixes Components

Four concrete mix types were developed for this research project; the first mix is regarded as a non-fibrous mix, as shown in Table 3. Various concrete mix designs were developed to improve compressive and splitting tensile strengths. Mix 3 has hybrid fibers (CA-PVA), with each type having a *Vf* of 0.6%. Mixes 2 and 4 have only one fiber type, CA and PVA, respectively. To achieve sufficient workability while maintaining strength, a high-range water reducer (HRWR), Sikament R4PN, was used. The mechanical properties of all mixes were assessed through experimental testing, with three cylinders and cube samples cast and tested for each blend to determine the average compressive and splitting tensile strengths.

3.2 Test Specimens

The tested beams are designed as rectangular concrete sections with dimensions (*b x t*) of 120×250 mm. The seven specimens were divided into three groups, designated as A, B, and C, as shown in Table 4. Group A comprises two

beams and was designed with a bottom steel ratio (s) of 1.45%. S1 is the controlled non-fibrous beam, and S2 contains CA fiber with (*Vf*) of 1.2%. Group B is reinforced with GFRP, with a reinforcement ratio (f) of 1.45% also, each beam is reinforced with a different type of fiber as shown in Fig. 4. Group B consists of S3, the controlled specimen; S4, reinforced with hybrid fiber (CA-PVA); S5, reinforced with PVA fiber; and S6, reinforced with CA fiber. Group C includes S2 as the controlled specimen, along with S6 and S7, in which the bottom reinforcement is a hybrid layer with s and f equal to 0.59% and 0.86%, respectively. Each beam in Group C contains *Vf* = 1.2% of CA fibers. All beams have top steel of *(2ϕ8)* as a stirrup hanger with vertical stirrups equal to *(10ϕ8/m)*. Group A comprises two beams (S1 and S2) designed to assess the effect of CA fibers on flexural performance, with HTS as the bottom reinforcement at the same ρ_s. Beam S2 is selected to be the control beam of the Group. Group B contains four beams (S3, S4, S5, and S6), which are set to determine the effect of PVA, CA, and hybrid fibers with different (*Vf*) on the flexural performance of the tested beams with a constant ratio of GFRP bottom reinforcement bars (*ρf*). for Group C, conrained S2, S7 and S6, S2 is considered the controlled beam for the group. Group C is designed to assess the effect of HTS, GFRP, and hybrid (GFRP-HTS) layers on the flexural performance of the tested beams, with a CA fiber content of 1.2% in each specimen.

The minimum fiber dosage in concrete depends on the specific application and the type of fiber used. For monofilament fibers, the dosage typically ranges from 0.03 to 0.1% by volume, and the maximum fiber dosage may reach 2% by volume [36–37]. In this study, the dosage is determined based on the average value of *Vf* (0.1–2.1%) to mitigate issues such as fiber balling, poor workability, and uneven distribution. Furthermore, the average dosage is used to reduce costs, as increased fiber content enhances performance but also increases costs and complicates the mixing process. Using a dosage below the recommended minimum may result in an inadequate fiber volume in the concrete mix, thereby yielding performance comparable to that of plain, unreinforced concrete rather than fiber-reinforced concrete.

3.3 Test Setup and Loading Technique

In the study, the beams are tested under load control with a uniformly distributed static load of capacity was 500 kN with a span from support to support equals 1700 mm and the total length of beams measured 1900 mm, as shown in Fig. 5. The loading rate is set to 0.5 kN/s to ensure a uniform crack distribution and to avoid localized failure (Hieu and Tuan 2021). As shown in Fig. 6, the load was uniformly distributed between two plates set 350 mm apart. The plate loads were symmetrically distributed about the beam centerline, and three LVDTs were set to measure the

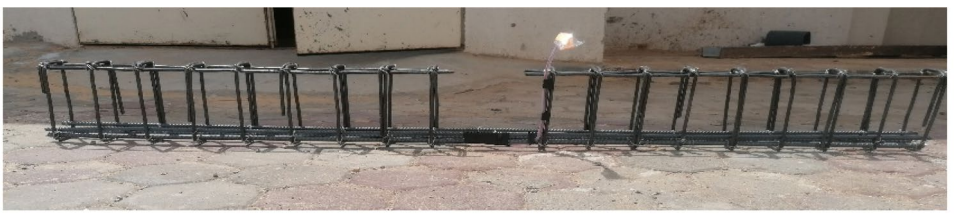

a) Reinforced Details For Group A

b) Reinforced Details For Group B

c) Reinforced Details For S7

Fig. 4 Reinforced Details for Tested Beams. **a** Reinforced Details For Group A. **b** Reinforced Details For Group B. **c** Reinforced Details For S7

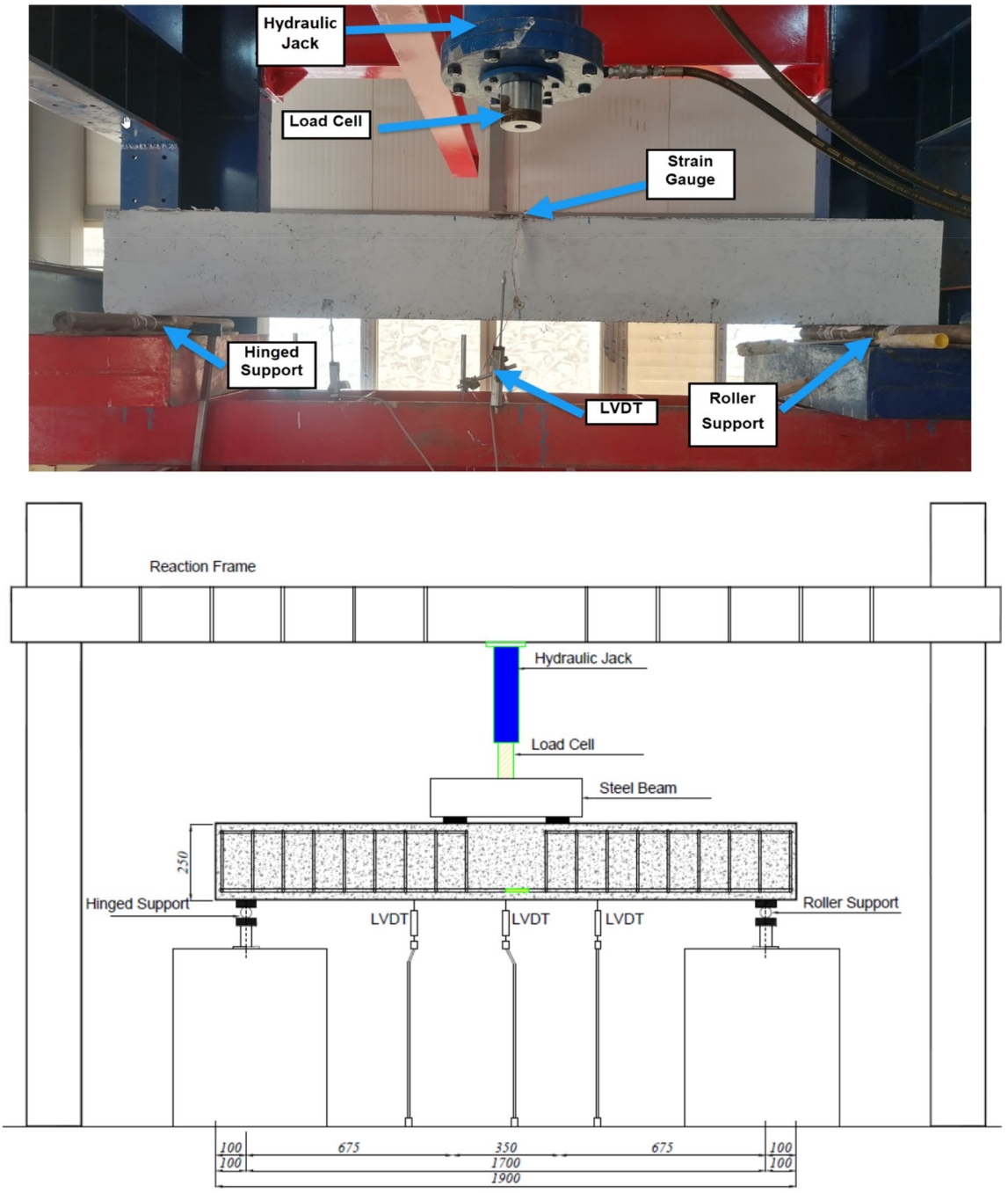

Fig. 5 Loading Technique and Test Setup

corresponding displacements. The beams are supported on the left by a roller and on the right by hinged supports to ensure their stability. During the initial loading process, the load is applied gradually to the steel plate, and it is then increased until the onset of crack propagation. Once the failure load is reached, the beam load is gradually reduced to prevent a local failure mode. For Group A, the strain gauge was placed on the lower steel bars, while for Group B, it was placed on the GFRP bars. Beam S7 comprised a hybrid layer of HTS-GFRP bar and was instrumented with two strain gauges: one attached to the HTS layer and one attached to the GFRP, enabling separate strain measurements for each constituent as shown in Fig. 6.

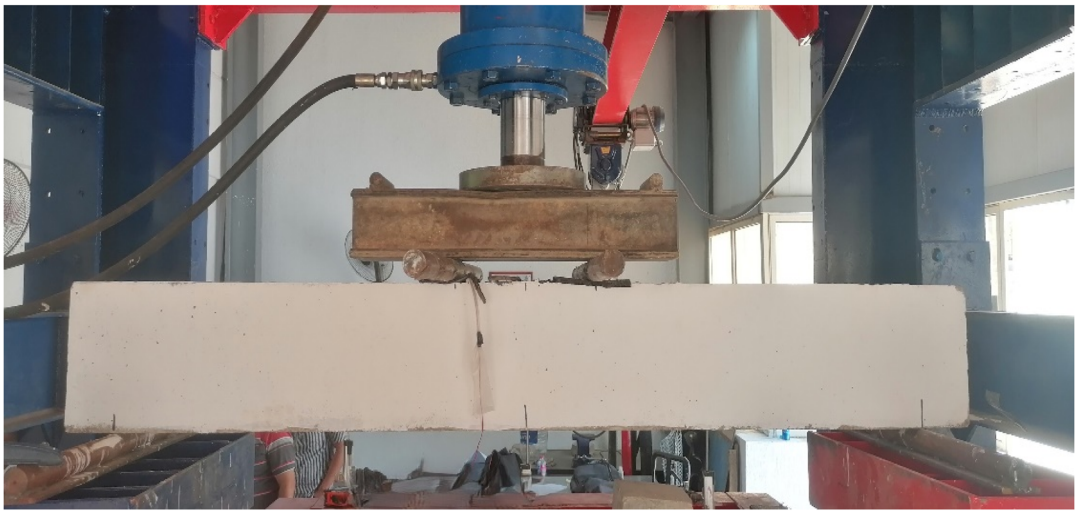

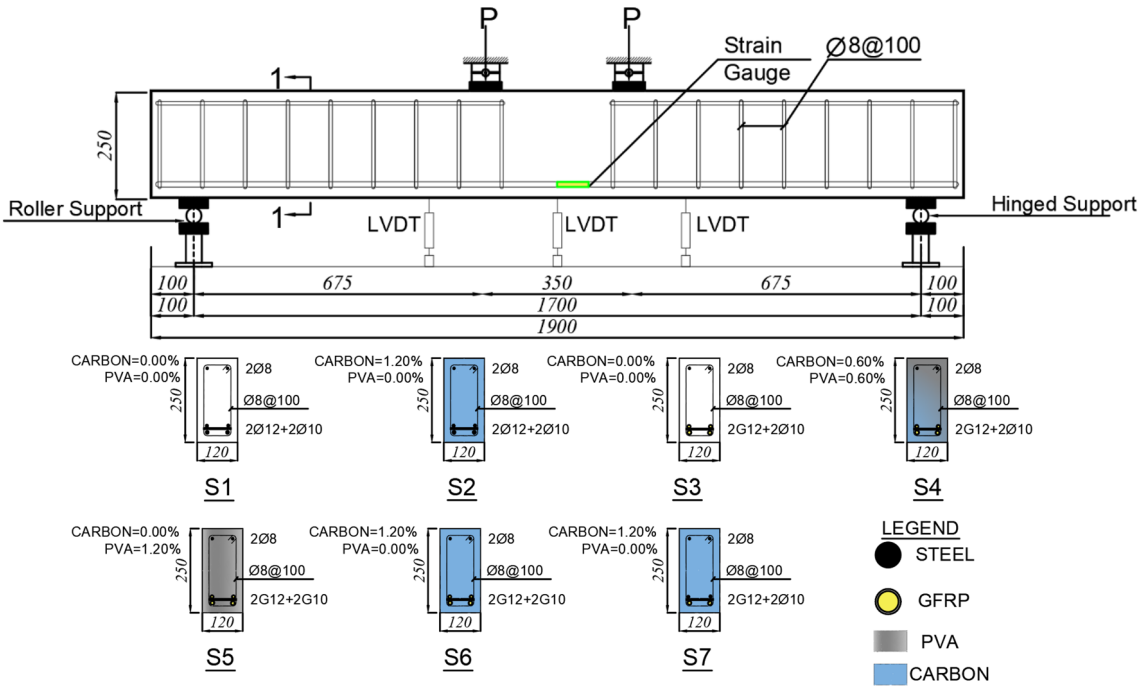

Fig. 6 Positions of Strain Gauges, LVDT, and Concrete Dimensions for Specimens

4 Results and Discussion of Experimental Works

4.1 Load-Deflection Performance Results

The load-deflection curves in Fig. 7 illustrate the beams' performance during testing and can be divided into three main stages. The first stage represents the elastic behavior of the specimens, which occurs before the initiation and propagation of the first cracks. The second stage occurs between crack formation and the yielding of the reinforcement bars, also known as the ultimate moment of resistance (from crack formation to yield). Lastly, the final stage shows strain hardening, in which deflection continues to increase with each load increment until the peak moment is reached.

For Group A, the failure load of S2, which includes CA fibers, is greater than that of S1 due to the higher tensile strength of the used fibers. Group B, S4, with hybrid fibers (CA-PVA), exhibits higher ductility and failure load compared to S3 due to the combined properties of CA and PVA fibers. For S5 and S6 with the inclusion of (Vf=1.2%) of PVA and CA fibers, the failure load was enhanced compared to S3. Group C, S6, reported a high failure load for S2 and

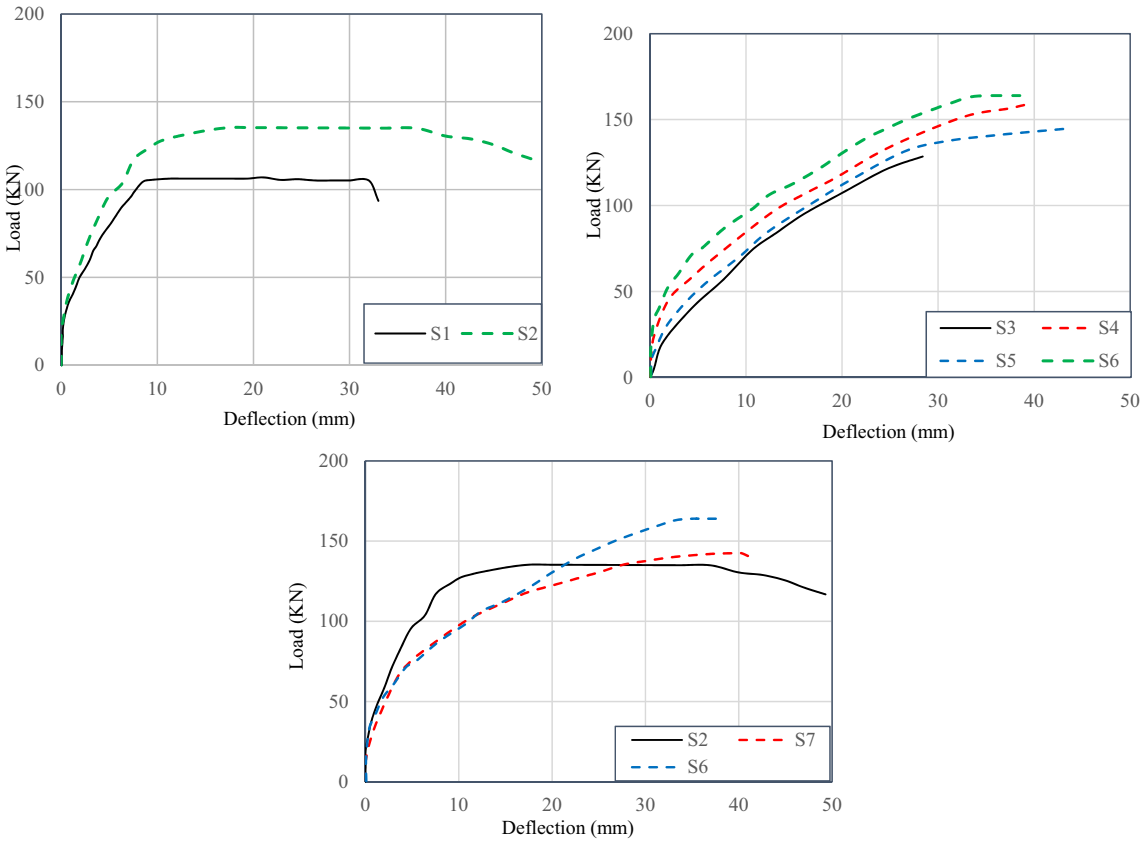

Fig. 7 Load-Deflection Curve for Tested Beams

S7, which was attributed to the high ultimate strength of the GFRP bars.

Regarding the deflection limit, for Group A, the displacement at yield increased by 32% and the displacement at the ultimate stage improved by 48% in S2 after inclusion of CA fibers. For Group B, hybrid (CA-PVA) fibers improved dy and du by 20% and 39%, respectively. For S5, using PVA improved displacement at the yield and ultimate stages by 7% and 53%, respectively. The previous result for S5 demonstrates the effectiveness of PVA in enhancing ductility across all stages, attributable to its high elongation. For S6, CA fibers improved dy and du by 36% and 38%, respectively. Group C (S2) exhibits a higher pre-failure deflection than S7 and S6. Deflection before failure reflects a decrease in ductility due to an increase in the GFRP reinforcement ratio, which reflects the effect of GFRP bars in reducing the ductility of HPRC beams. The Experimental results have emphasized the contributions of CA and PVA fibers in enhancing the ductility index of beams with varying proportions of HTS and GFRP bars. Figure 7 shows that the experimental load-deflection curves facilitate the following measurements:

4.1.1 Yield and Ultimate Flexural Loads

The experimental yield (*Py*) and maximum (*Pu*) flexural loads were recorded and reported during testing, with all data presented in Table 5. In general, the addition of short fibers into concrete mixtures increases the values of (*Py*) and (*Pu*). For Group A, compared to beam S1, (*Py*) was improved by 51% within the inflection of CA fibers. For the ultimate flexural load, using *Vf* equals 1.2% of CA increased (*Pu*) by a ratio of 26%, as a result of the high efficiency of CA fiber in the concrete matrix. For Group B, compared to S3, the increase ratios of (Py) were 36%, 14%, and 57% for S4, S5, and S6, respectively. Regarding load at the ultimate stage (Pu), using PVA fibers in S5 enhanced (Pu) by 12%. For S4 and S6, where hybrid (CA-PVA) and CA fibers were used, the improvement of (Pu) was 24% and 27%, respectively. Moreover, the significant increase in ultimate flexural loads in S4 and S6 is attributed to the high elastic modulus of CA fibers, which enhances the flexural properties of the concrete beams. For Group C, referring to S2, using a hybrid layer of HTS and GFRP improved (*Pu*) by 6%; however, the yield flexural load decreased by 17%. For S6, the presence of GFRP bars with (ρf) equal to 1.45 improved (Pu) by 21%, which is a result of the high value of

Table 5 Experimental Results for the Tested Beams

Group	Beam	Experimental Test Results								Relative Experimental Results to the Control Beams							
		P_{cr} (KN)	P_y (KN)	δy (mm)	P_u (KN)	δu (mm)	Ka (KN/m)	Kp (KN/m)	I (KN.mm)	DF	$\frac{P_{cr}}{P_{cr-R}}$	$\frac{P_y}{P_{y-R}}$	$\frac{\delta y}{\delta y-R}$	$\frac{P_u}{P_{u-R}}$	$\frac{\delta u}{\delta u-R}$	$\frac{Ka}{K_{aR}}$	$\frac{Kp}{K_{pR}}$	$\frac{DF}{DF_R}$
A	S1*r*	48	74.9	5.7	107	32	13.14	5.1	3181	5.61	1.00	1.00	1.00	1.00	1.00	1.00	1.00	1.00
	S2	78	113	7.5	135	47.2	15.07	8.2	6071	6.29	1.63	1.51	1.32	1.26	1.48	1.15	1.61	1.12
B	S3r	28	57.2	6.8	128.5	28.4	8.41	4.2	2510	4.18	1.00	1.00	1.00	1.00	1.00	1.00	1.00	1.00
	S4	38	70.6	7.1	159.3	39.6	9.94	5.1	3587	4.89	1.36	1.36	1.19	1.24	1.39	1.18	1.21	1.17
	S5	32	73.5	8.1	144.5	43.5	9.07	4.5	4221	5.96	1.14	1.14	1.07	1.12	1.53	1.08	1.07	1.43
	S6	44	77.78	7.3	163.8	38.5	10.65	5.8	4120	5.27	1.57	1.57	1.07	1.27	1.36	1.27	1.38	1.26
C	S2*r*	78	113	7.5	135	47.2	15.07	8.2	6071	6.29	1.00	1.00	1.00	1.00	1.00	1.00	1.00	1.00
	S7	54	94.2	7.05	142.5	40.29	13.36	5.2	4704	5.71	0.69	0.83	0.94	1.06	0.85	0.89	0.63	0.77
	S6	44	77.78	7.3	163.8	38.5	10.65	5.8	4120	5.27	0.56	0.69	0.97	1.21	0.82	0.71	0.71	0.68

ultimate tensile strength of GFRP bars. On the other hand, compared with S6 using GFRP bars, S2 with HTS has a 21% higher yield flexural load. Therefore, it is concluded that GFRP bars enhance only the ultimate stage, while HTS bars enhance the yielding stage.

4.1.2 Yield and Post-Cracking Stiffnesses

The yield stiffness (*Ka*) is defined as the ratio of the flexural yield load (*Py*) to the Corresponding displacement (*δy*). S2 exhibited a 15% increase in yield stiffness relative to S1. For Group B, referring to S3, (*Ka*) increases by 18% after using hybrid (CA-PVA) fibers with 0.6% *Vf* in S4. The inclusion of PVA and CA fibers in S5 and S6 improves the yield stiffness by 8% and 27%, respectively. S5 showed a slight enhancement due to the lower elastic modulus of PVA fibers. For Group C, referring to S2, the use of a hybrid reinforcement layer reduced *Ka* by 10% for S7, and increasing $(\rho_{fj}$ led to a reduction in yield stiffness from 15.07 to 10.65, which reflects the effect of GFRP in lowering the yield stiffness.

The post-cracking stiffness (*Kp*) could be deduced from the load-deflection curve region after the onset of the first cracking formation. Group A's post-cracking stiffness increased by 61% for S2 after the inclusion of CA with (*Vf*) of 1.2%, which reflects the reinforcing effect of CA fibers in the cement matrix. For Group B, the post-cracking stiffness was enhanced by 21% after using hybrid (CA-PVA) fibers for S4 and 38% with the inclusion of CA fiber in S6. However, for S5, with the usage of PVA fiber, the post-cracking stiffness was enhanced by 7%. It indicates a more significant effect of CA fibers on post-cracking stiffness after the first crack propagation than PVA fibers. The strength of CA fibers derives from their high tensile strength. Compared with S2, replacing HTS with GFRP bars with the same reinforcement ratio in S6 reduced the post-cracking stiffness by 18%, which explained the effect of GFRP on post-cracking stiffness in Group C. Moreover, the usage of a hybrid layer of HTS and GFRP in S7 reduced (*Kp*) by 29%.

When comparing the enhancement values of *Ka* and *Kp*, it is evident that the effects of short fibers are primarily observed in the post-cracking phase, as indicated by the slightly smaller enhancement ratios in *Ka*. The high tensile strength and ductility indicate the positive effect of short fibers in the post-cracking stage.

4.1.3 Ductility Factor (DF)

The Ductility Factor (DF) is essentially the ratio of deflection at the ultimate level (*δu*) to the deflection corresponding to yield load (*δy*) (Shanour et al. 2018) and (Pakravan et al. 2016). In Group A, the use of CA fibers enhanced ductility by 12% in S2 compared to the controlled beams in S1. For

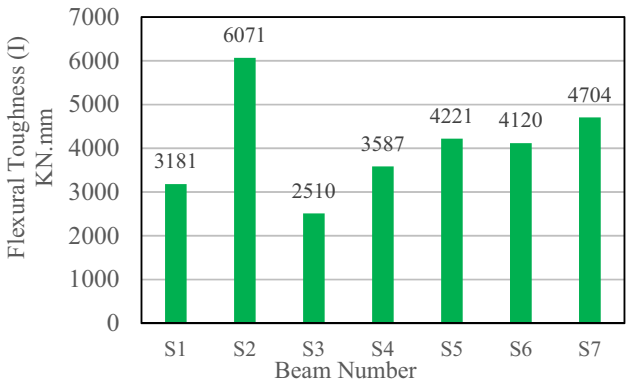

Fig. 8 Flexural Toughness for RC Beams

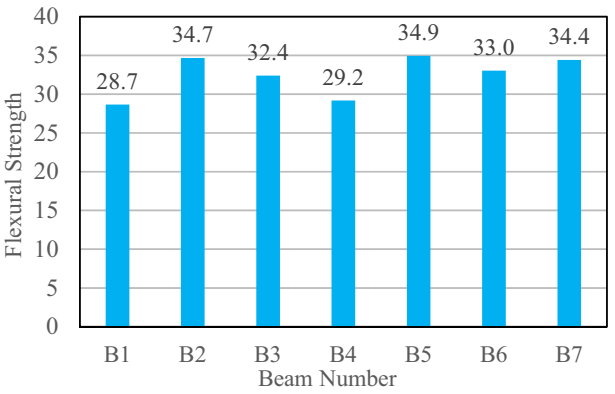

Fig. 9 Flexural Strength for RC Beams

Group B, referring to S3, the ductility factor was increased by 17% with the addition of hybrid (CA-PVA) fibers in S4. (*Df*) enhanced with inclusion of *Vf* with 1.2% of PVA and CA in S5 and S6 with ratios of 43% and 26%, respectively. The slight increase in S2 and S6 is due to the effect of CA fibers in S2 and the double impact of GFRP bars with CA fibers in S6, which has a limited effect on ductility. However, the considerable enhancement in S4 and S5 is attributable to the presence of PVA fibers with high elongation, which increases ductility. For Group C, compared with S2, using ρf=0.86% reduced ductility by 23% in S7, whereas increasing ρf to 1.45% reduced *Df* by 30%. This provides evidence of the effectiveness of HTS in enhancing ductility and detecting incipient cracks before failure.

4.1.4 Flexural Toughness (I)

The magnitude of flexural toughness (I) is defined as the area beneath the load-deflection curve. It depends on the relationship between the ultimate load (Pu) and the deflection at the ultimate load (δu). Toughness is regarded as a touchable measure of ductility. For Group A, compared to S1, the inclusion of CA fibers in S2 enhanced (I) by 91% as per Fig. 8. In Group B, the toughness of S4 has an enhancement ratio of 43% compared to S3. With the usage of PVA fiber in S5, the toughness increased by 68%. The inclusion of CA fiber improved toughness by 64% in S6 compared to S3. The 64% increase in toughness in Group A, compared with other Groups, was attributable to the effect of HTS on ductility. Moreover, it was found that PVA fibers are more effective in flexural toughness than CA fibers due to the high tensile elongation of PVA fibers. For Group C, compared with S2, flexural toughness decreased by 23% in S7, which incorporated hybrid layers (GFRP-HTS) into the bottom reinforcement. Also, after using GFRP bars with (ρ_f) equal to 1.45%, toughness decreased by 31% as per S6 with respect to S2. It is noted that GFRP bars reduce ductility, thereby adversely affecting flexural toughness.

4.1.5 Flexural Strength

The flexural strength of the beam was found from the following formula PuL/bt^2, where the concrete dimensions of the beam were bxt in mm, L is the length of the beam measured from center to center between supports in m, and Pu is the ultimate flexural load in kN. For Group A, there is a noticeable improvement in S2 by 21% compared to B1, as shown in Fig. 9. For Group B, adding PVA fibers in S5 with (*Vf*=1.2%) enhanced flexural strength by 13%. The inclusion of hybrid (CA-PVA) fibers in S4 and CA fibers in S6 increased flexural strength by 24% and 27%, respectively. The enhancement ratios in the presence of CA fibers are more than those of PVA fibers, which explains the ability of CA fibers to affect the ultimate stage. For Group C, the flexural strength was increased by 2% due to the inflection of hybrid bar layers in S7. After replacing the HTS with GFRP bars in S6, the flexural strength increased by 20% compared with S2. From previous results, GFRP bars in hybrid layers enhance flexural strength, and rising (ρf) led to a considerable Enhancement in flexural strength.

4.2 Strains in Steel and GFRP Bars

Strain gauges were placed on the mid-bottom longitudinal reinforcement bars of all the specimens being studied, as shown in Fig. 6. Figure 10 illustrates the load-strain relationship from these bottom longitudinal rebars. The ultimate strain (εu) values for the HTS and GFRP bars are presented in Table 6. The ultimate strain of the HTS bars was higher than the yielding strain of the bars, which supports the observation that the steel bars yielded before the beams failed. Moreover, the ultimate strains for GFRP bars in S3, S4, S5, S6, and S7 are measured at 0.0125, 0.0154, 0.0147, 0.017, and 0.0187, respectively. All these values are below the maximum ultimate strain of 0.02, which proves that rupture failure of GFRP bars has been avoided. The failure of beams S1, S2, and S7 with HTS and hybrid layers

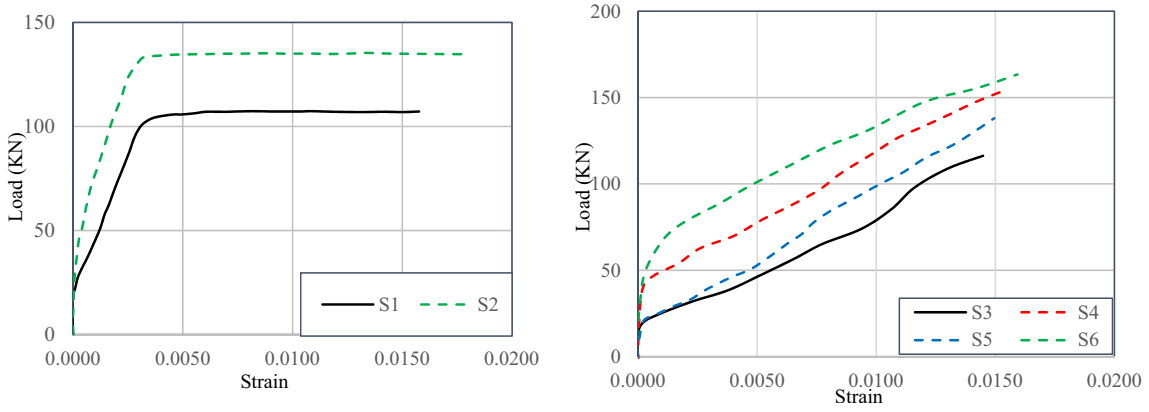

Fig. 10 Load-Strain Curves of Longitudinal Reinforcement of Tested Beams

Table 6 Tensile strains of HTS and GFRP bars

Beam	Yield and Ultimate strains of HTS and GFRP bars			
	Rebars Type	εy	εu	Strain Ductility μs
S1	HTS	0.002	0.0158	7.9
S2	HTS	0.002	0.018	9.0
S3	GFRP	0.0036	0.0125	3.5
S4	GFRP	0.0041	0.0154	3.8
S5	GFRP	0.004	0.0147	3.7
S6	GFRP	0.0045	0.017	3.8
S7	HTS	0.002	0.0215	10.8
	GFRP	0.0048	0.0187	3.9

was ductile, characterized by steel yielding and subsequent strain, followed by concrete crushing. In contrast, the failure of beams with GFRP bars (S3, S4, S5, and S6) was due to compression failure, which occurs when the concrete crushes without prior warning. Compression failure occurs due to the high percentage of GFRP bars, which increases the beams' strength and brittleness.

For Group A, the ultimate strains for S2, where CA fibers were included, were equal to 0.018, which is 13% higher than that of S1. Consequently, beams with CA and hybrid fibers exhibited a high warning level before failure. Referring to S2, the ultimate steel strain increased by 19% for S7, indicating that the hybrid layers of (GFRP-HTS) can provide a high warning level during failure. For Group B, strain ductility (μs) was lower than in other groups due to GFRP bars, as shown in Table 6.

4.3 Experimental Failure Mode Shapes and Crack Patterns

A key approach to characterizing failure modes is to monitor crack propagation while recording the loads applied at different stages of testing. This is an essential method for evaluating the effects of various parameters on the overall performance of the tested beams. Crack patterns and failure modes of the tested beams are shown in Fig. 11. During loading, cracks developed at the mid-span of all beams, where the moment was highest. With additional load, cracks propagated from the mid-span toward the ends of the beams. With increasing loads, the cracks located at the uplifted area of maximum moment became larger and deeper, ultimately leading to failure. The failure mechanism of the tested beams was flexural tension, characterized by the yielding of the steel reinforcement, followed by concrete crushing, and ultimately, the rupture of the GFRP bars. Beams with HTS and hybrid layers (GFRP-HTS) of reinforcement bars exhibited a tension failure type, characterized by the yielding of tensile steel bars; however, beams with GFRP bars displayed compression failure, accompanied by concrete cracking in the compression zone, as shown in Fig. 11. The compression failure are clearly noticed in S3, S4, S5 and S6 where GFRP used with (ρ_{fj} equal to 1.45% which provides more brittleness for the tested beams.

For Group A, referring to S1, using CA fiber within S2 delayed crack formation by 63%, indicating the effect of CA fibers in limiting crack spreading. Compared to S3, the cracking propagation was delayed by 36% by the inclusion of hybrid (CA-PVA) fibers in S4. PVA fibers with (Vf = 1.2%) have limited crack propagation by 14% as in S5. For S6, compared with S3, CA fibers exhibit a 57% reduction in crack-propagation delay. As a result, the beams exhibited improved ductility and toughness, leading to an enhanced load-bearing capacity and a reduced likelihood of sudden brittle failure. For Group C, as referenced in S2, using a hybrid layer (GFRP-HTS) and GFRP reinforcement bars in S7 and S6 accelerated the formation of cracking.

4.4 Summary of Results

Generally, the effect of CA-fiber can be presented in Fig. 12. The inclusion of carbon fibers (CA-fiber) increased the yield load (Py) by 44% and the ultimate load (Pu) by 27%. This improvement can be attributed to the high tensile

S1

S2

S3

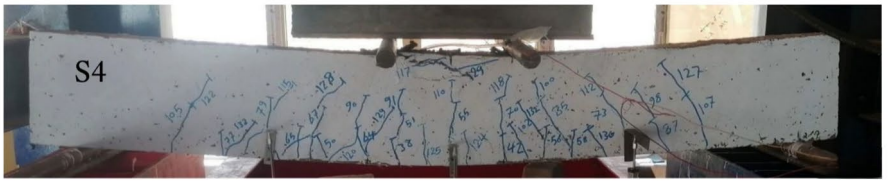

S4

S5

S6

S7

Fig. 11 Failure Mode Shapes and Crack Patterns for Tested Beams

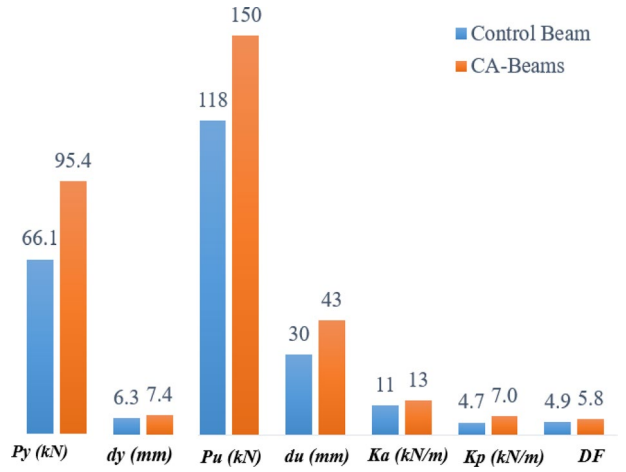

Fig. 12 Effect of CA Fibers

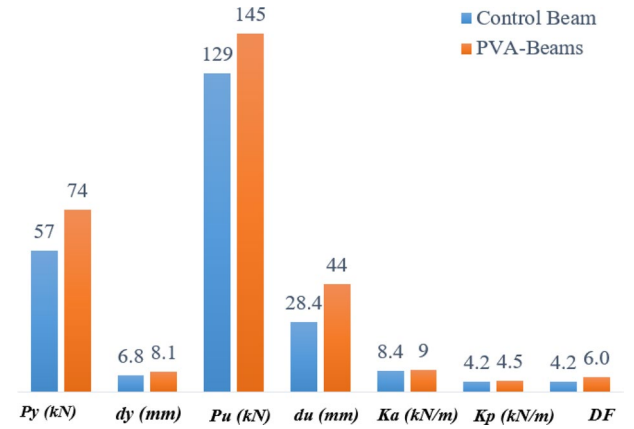

Fig. 13 Effect of PVA Fibers

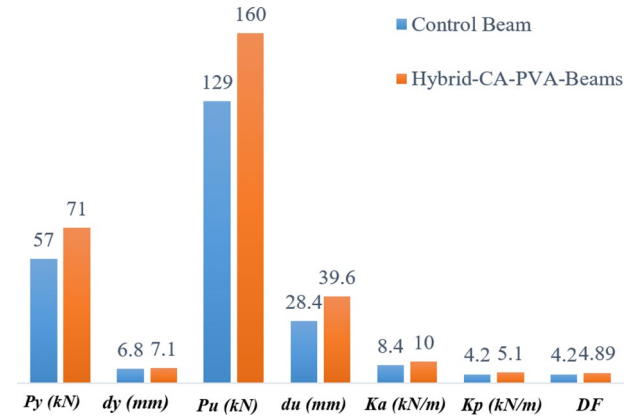

Fig. 14 Effect of Hybrid Fibers

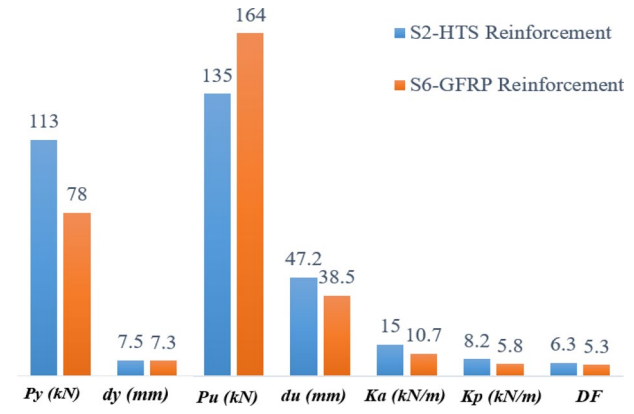

Fig. 15 Effect of GFRP Reinforcement

strength of the fibers, which enhances the concrete's tensile strength and, consequently, its resistance to flexural loads. For displacement at the yield and ultimate stages, CA-fiber increased δy and δu by 18% and 43%, respectively. Additionally, CA-fiber increased yield and cracking stiffness by 18% and 50%, respectively. The significant enhancement in Kp is attributable to the post-cracking effect of the CA fiber. *DF* increased by 18% through the incorporation of CA-fiber into concrete mixtures, as the fibers increase the beam's flexural capacity, thereby delaying crack propagation and increasing ductility.

The effect of PVA fiber is shown in Fig. 13; compared with control beams, the yield and ultimate flexural loads increased by 28% and 13%, respectively. Under the ductility condition, deflections at the yield and ultimate stages increase by 19% and 53%, respectively. The significant increase in deflection is due to the high elongation of PVA fibers, which provide strain hardening during loading. PVA fibers improved the yield and cracking stiffness by 8% and 7%, respectively. Ductility is increased by 43% with the incorporation of PVA fibers, owing to their high tensile strength, which delays crack formation and thereby improves ductility. The hybrid fiber matrix effect is shown in the figure. 14. The inclusion of hybrid (CA-PVA) fibers improved *Py* and *Pu* by 25% and 24% respectively. It would be explained by the high Young's modulus of CA fibers and the tensile strength of PVA fibers. For the displacements at the yield and ultimate stages, hybrid fibers increased δy and δu by 5% and 39%, respectively. The high initial-to-cracking-stiffness ratio could explain this; hybrid fibers increased *Ka* and Kp by 19% and 21%, respectively, as shown in Fig. 14. The ductility factor of the hybrid matrix increased by 17% due to the elongation of PVA fibers.

The effect of using GFRP bars instead of HTS with the same reinforcement ratio is clearly shown in Fig. 15. As shown, GFRP bars reduced the yield load by 31%, whereas the ultimate load increased by 22%. The higher ultimate strength of GFRP bars accounts for this. For the displacements at the yield and ultimate stages, δy and δu decrease by 2% and 18%, respectively. For the ductility factor, using GFRP bars with $\rho f = 1.45\%$ reduces it by 16%, as GFRP bars enhance the brittleness of concrete beams.

The effect of the hybrid reinforcement layer ($\rho_{f=}$ 0.86% & $\rho_{s=}$ 0.59%), versus HTS ($\rho_{s=}$ 1.45%), is shown in Fig. 16.

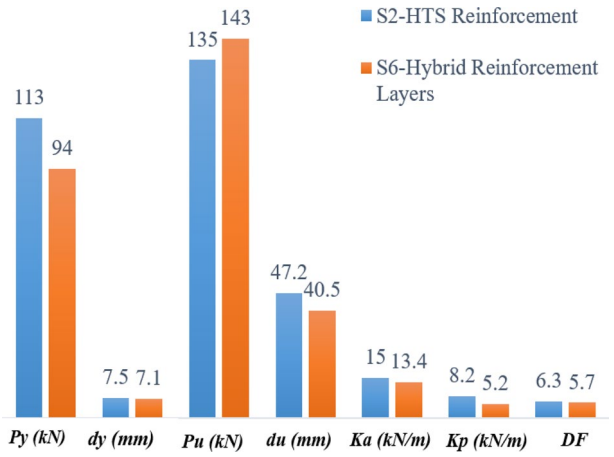

Fig. 16 Effect of Hybrid Fibers

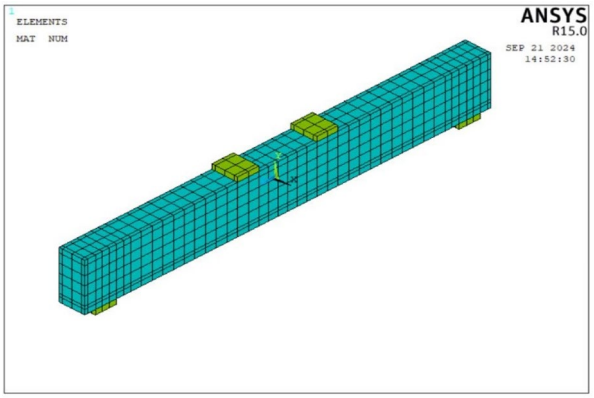

Fig. 17 Simulation of Concrete Material of Tested Beams by Solid 65

The hybrid layer has an adverse effect on *Py* by 16%; on the other hand, *Pu* increased by 10%. Under the ductility condition, the inflection of the hybrid layers reduced δy and δu by 5% and 14%, respectively. That explained the effect of the hybrid layer on the ductility. The hybrid reinforcement layer reduced the ductility factor *(Df)* by 9.5%, as GFRP bars reduced ductility by increasing the ultimate load and allowing crack propagation due to increased brittleness.

5 Numerical Finite Elements analysis

A numerical finite element analysis (NFEA) was performed to validate the experimental results obtained from the tested beams. The finite element analysis package used is ANSYS 15.0 (ANSYS 2009), a commercially available software. The load-deflection curve is crucial for characterizing the behavior of RC beams. The curve indicates the parameters: the flexural load at yielding (*Py*), the corresponding deflection (*δy*), the load capacity at failure (Pu), and the corresponding ultimate deflection (*δu*).

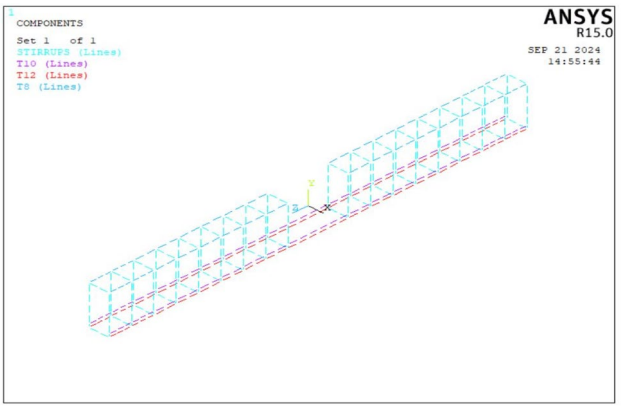

Fig. 18 Simulation of Reinforcement of Tested Beams by Link 180

5.1 Finite Element Geometry and Materials Simulation

For geometric idealization, a 3-D numerical finite element software was used to model the seven RC beams. The concrete material was modeled using 3D Solid 65, which consists of eight nodal points, as shown in Fig. 17. Solid 65 can deform either elastically or plastically, and can also crack and crush. The reinforcement bars and shear links were modeled using 3-D elements (Link 180) in Fig. 18. Link 180 can carry a plastic deformation and has two end nodes, each with three degrees of freedom. In this case, point loads were applied to two plates, which acted as supports for the beams. All plates were modeled as 3D solids to prevent stress concentration, given their high stiffness.

A 3-D finite element analysis tool was used to simulate seven reinforced concrete beams through geometric idealization. The concrete was modeled using Solid 65, which is characterized by 8-nodal points, as shown in Fig. 17. This element is adept at capturing both elastic and plastic deformations, as well as simulating cracking and crushing patterns. As depicted in Fig. 18, HTS, GFRP bars, and vertical stirrups were modeled using 3-D Link-180 elements. Link 180 can accommodate plastic deformation and consists of two end nodes, each with three degrees of freedom. Point loads were applied to two plates that supported the beams. To mitigate potential stress concentration issues, all plates were modeled as 3D solid elements with 185 elements, due to their significant stiffness.

5.2 Comparison of Crack Patterns and Load-Deflection

The results of the Numerical Finite Element Analysis (NFEA) were also compared between the crack configurations observed experimentally and those predicted numerically for all crack patterns. Figure 19 compares the

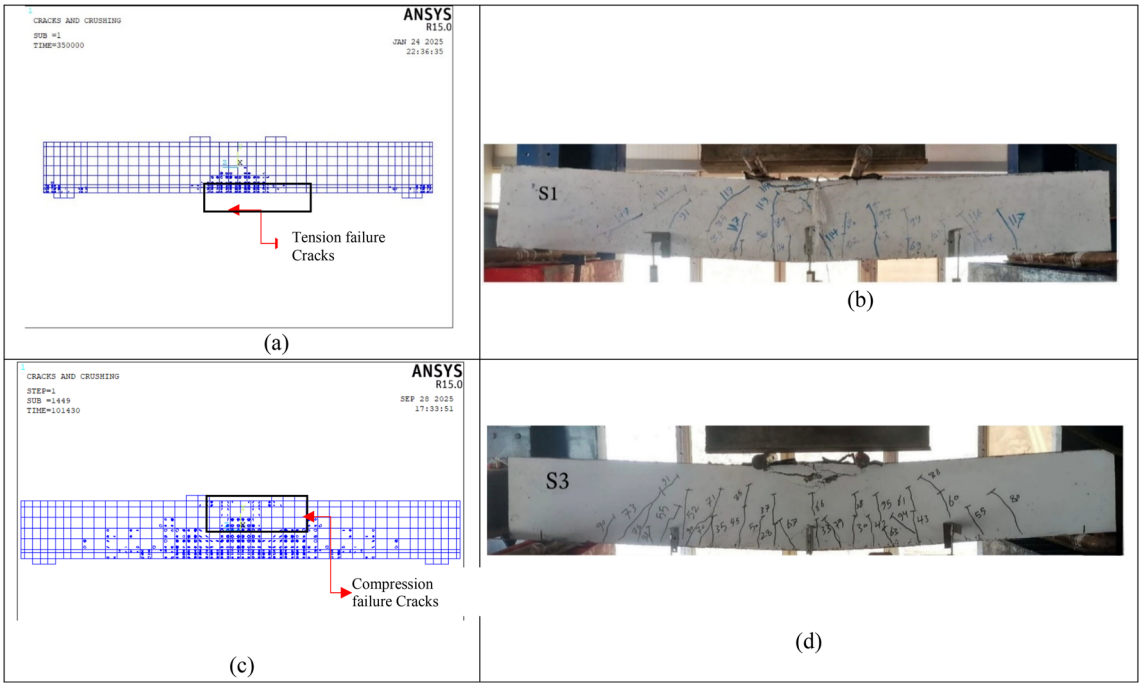

Fig. 19 Crack Patterns Verification for S1 and S3. **a** Crack Pattern from NFEA For S1. **b** Experimental Crack Pattern For S1. **c** Crack Pattern from NFEA For S3. **d** Experimental Crack Pattern For S3

experimental crack patterns with the numerically predicted ones for beams S1 and S3. Most numerical results showed good agreement with the experimental results. Comparisons of the numerical load-deflection curves with the experimental load-deflection curves of the test beams are given in Fig. 20. The average ratio of the yielding load [*Py*, *exp./Py*, *NA*.] was 1.053. The standard deviation was 0.118, and the coefficient of variation was 10.62%. The mean deformation ratio corresponding to the yield point [*δy*, *exp./δy*, *NA*.] was 1.0314, with a standard deviation of 0.15 and a coefficient of variation of 14.6%. For the ultimate stage, the average ratio [*Pu*, *exp./Pu*, *NA*.] equals 0.967. The mean average deflection was [*δu*, *exp./δu*, *NA*.] is 1.114. The comparison of the predicted results from NFEA with the experimental test results showed a satisfactory correlation, as depicted in Table 7.

6 Nominal Flexural Strength

Strain compatibility analysis is a method for comparing *Mexp*. with *Mn*. The nominal moment capacity of the rectangular beam of high-performance hybrid fiber-reinforced concrete (HPRC) section (b × t) has been computed. ACI 318−19 (ACI 318 et al. 2019) predictive formula will be considered an extension of the formula provided in this code. Nonetheless, reasonable assumptions were made in estimating the nominal moment capacity. Furthermore, this formula accounts for the ideal stress-strain curves of steel and GFRP bars, taking into account the influence of composite fibers on the tension side. A simplified rectangular stress block in Fig. 21 depicts reinforcement combinations, namely steel bars, GFRP bars, and hybrid fibers (acting in high-performance concrete), so that the equilibrium can now be expressed as:

$$Cc = T_s + T_{GFRP} + T_f \tag{1}$$

The concrete compression force of high-performance (Cc) can be estimated using the rectangular stress block in the following manner:

$$Cc = \text{o'}_{f.c} * A_c \tag{2}$$

The compressive strength of RC beams with hybrid fibers ($o'_{f.c}$) can be determined as:

$$o'_{f.c} = \alpha \,.\, f\prime_{c\,(exp.)} \tag{3}$$

The parameter (α) has been adopted as 0.85 in accordance with ACI Code 318−19 (ACI 318 et al. 2019). Additionally, the cylindrical compressive strength of HPRC beams containing hybrid fibers has been measured *f'c(exp)*. Furthermore, the area of the compression zone (Ac) is given in the following manner:

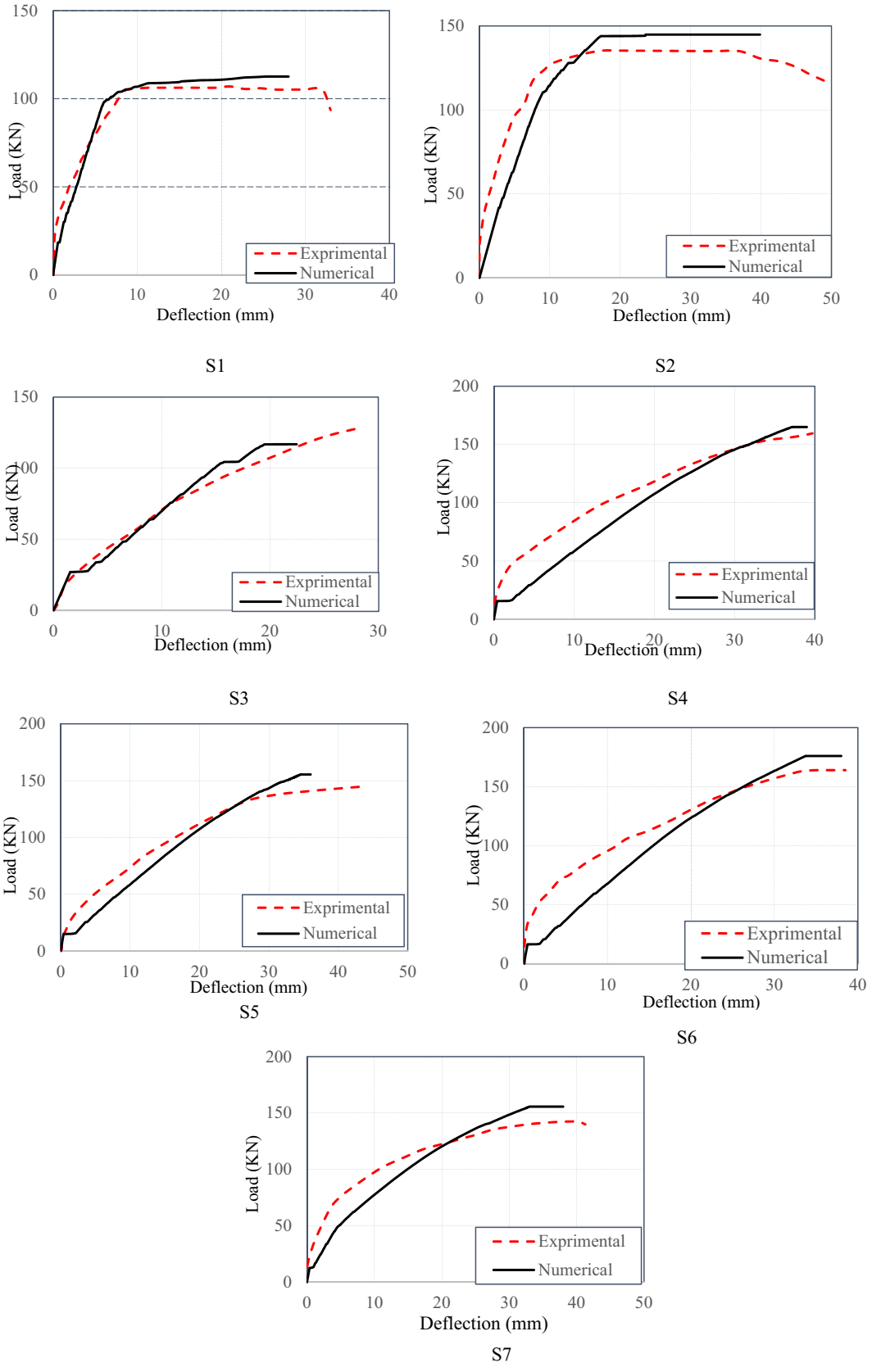

Fig. 20 NFEA and Experimental Load-Deflections Verification

Table 7 Hyper parameters

Beam	Experimental test results			NFEA results			Experimental results/NFEA results		
	P_y (KN)	d_y (mm)	P_u (KN)	d_u (mm)	P_y (KN)	d_y (mm)	P_u (KN)	d_u (mm)	$\frac{Py-exp}{Py-NA.}$	$\frac{\delta y-exp}{\delta y-NA.}$	$\frac{Pu-exp}{Pu-NA.}$	$\frac{\delta u-exp}{\delta u-NA.}$
S1	74.9	5.7	107	32	84	6.1	112	28	0.89	0.93	0.96	1.14
S2	113	7.5	135	47.2	109	8.8	144	40	1.04	0.85	0.94	1.18
S3	57.2	6.8	128.5	28.4	64	5.8	116	24	0.89	1.17	1.11	1.18
S4	70.6	7.1	159.3	39.6	59	6.2	165	39	1.20	1.15	0.97	1.02
S5	73.5	8.1	144.5	43.5	67	6.8	155	36	1.10	1.19	0.93	1.21
S6	77.78	7.3	163.8	38.5	69	6.5	175	38	1.13	1.12	0.94	1.01
S7	94.2	7.05	142.5	40.29	84	8.7	155	38	1.12	0.81	0.92	1.06
Average									1.05	1.03	0.967	1.114
Standard Deviation									0.12	0.15	0.060	0.077
Coefficient of variation									10.62%	14.90%	6.25%	6.88%

$$A_c = b.\, a \tag{4}$$

The effective depth of the compressive zone (a) was estimated as:

$$a = \beta\, .\, C \tag{5}$$

The factor (β) should follow the upper and lower limits of $0.65<\beta<0.85$ (ACI 318 et al. 2019), which are determined from the Eq. 6:

$$\beta\ = 0.85 - 0.05\ \left[\frac{f'_{c\,(exp.)} - 28}{7}\right] \tag{6}$$

Conclusively, Cc can be computed as:

$$Cc = 0.85 * f'_{c\,(\exp.)} * b * a \tag{7}$$

For the tension zone, tension force in HTS bars, GFRP bars T_S, and T_{GFRP} can be computed as follows:

$$T_s = f_y * A_s \tag{8}$$

$$T_{GFRP} = f_{GFRP} * A_{GFRP} \tag{9}$$

The short fiber tension force due to CA, PVA, and hybrid (CA-PVA), known as (T_{fibers}), can be determined as follows:

$$T_{fibers} = o'_{fibers} * A_{fibers} \tag{10}$$

Short Fibers concrete Area in the tension side (A_{fibers}) can be defined as follows:

$$A_{fibers} = b\ x\ e \tag{11}$$

The distance from the extreme tension fiber to the neutral axis of the stress block (e) can be defined as follows:

$$e = \ t - \frac{(\epsilon_{\ Fiber} + 0.003)\ C}{0.003} \tag{12}$$

Another equation to calculate (e) in terms of the depth of the rectangular block (a) is predicted as follows:

$$e = t - \ \frac{a}{0.9\ \beta^{\,2}} \tag{13}$$

The fibrous tensile concrete strength (O_{fibers}) can be predicted as (ACI 318 et al. 2019) :

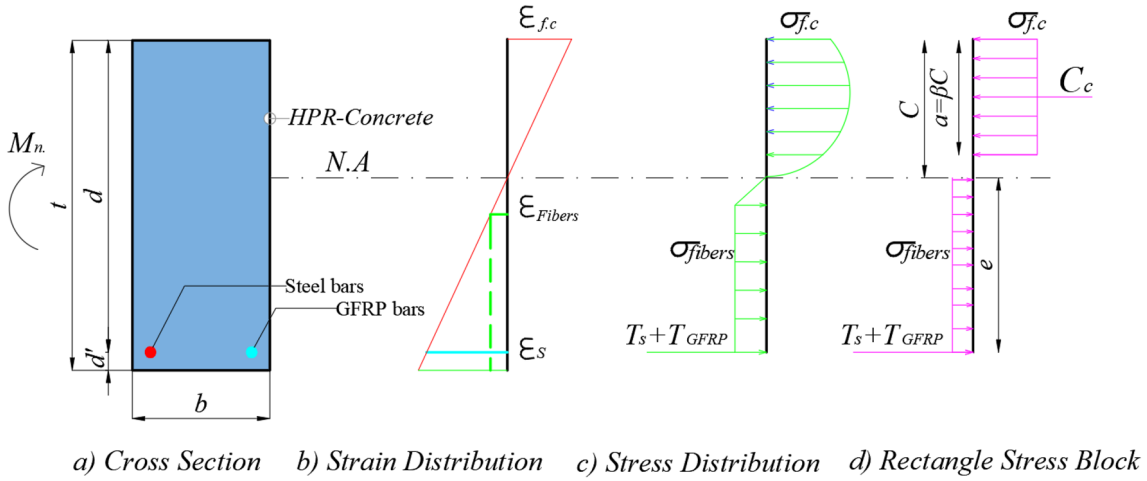

Fig. 21 Stress Distribution for Hybrid Fiber RC Beams Cross Section

$$o'_{fibers} = 0.00772 \frac{l_f}{\Phi_f} V_F F_{be} \left(\frac{e}{t}\right) \quad (14)$$

Where Fbe is the bond efficiency, it is chosen to equal 1, and *Vf* is the volume of fibers.

Accordingly, $M_{n.}$ can be estimated as:

$$M_{n.} = \left[(A_s f_y + A_{GFRP} f_{GFRP})\left(d - \frac{a}{2}\right)\right] + \left[o'_{fibers} b\ (e)\left(\frac{e}{2}\right)\right] \quad (15)$$

Table 8 presents a comparison of the experimental and nominal flexural strengths, indicating a strong correlation between the two. The average ratio of [M, exp./Mn.] for the beams evaluated in this study is 0.97, with a standard deviation of 0.068, and a coefficient of variation of 6.95%. In addition, Table 8 compares 38 reinforced concrete beams tested in studies (Shanour et al. 2018, Meng et al. 2017, Ge et al. 2020, Ge et al. 2019) that employed hybrid or single fibers with various (*Vf*) ratios and various reinforcement ratios of GFRP or HTS. The average ratio of [M, exp./Mn.] is 0.97, with a standard deviation of 0.101, and a coefficient of variation of 10.4% as shown in Fig. 22.

7 Discussions and Conclusion Points

An assessment of the flexural performance of beams reinforced with carbon, PVA, or a hybrid of both fibers was conducted. The experimental results were rigorously assessed and described in sufficient detail. Also presented is a comparison of the predicted or nominal results to those obtained by NFEA, as follows:

1) The use of CA fibers increases the yielding and ultimate performance of the tested beams, mainly due to their high Young's modulus and the highest aspect ratio (*lf/ϕf*). A noticeable improvement of around 59% and 28% was observed in the yielding and ultimate flexural load for beams with CA fibers. Similarly, the use of hybrid fibers produced increases of 32% and 22% for (Py) and (Pu), respectively. Beams with PVA fibers yielded the required improvements; however, these beams exhibited the most significant deflections due to PVA fiber elongation, resulting in pronounced strain hardening. GFRP bars also increased the ultimate capacity stage of the beams by 21%.
2) Short fibers' tensile strength leads to increased yield stiffness, while high elongation values lead to improved post-cracking stiffness. For beams with CA and hybrid fibers, the yield stiffness was 27% and 18% higher, respectively. However, GFRP bars result in a 20% decrease in yield stiffness due to decreased energy dissipation under loading. Improvements in post-cracking stiffness were observed for the CA fiber by 38% and for the hybrid (CA-PVA) fiber by 21%. Conversely, GFRP bars decreased post-cracking stiffness when compared with HTS bars by 18%.
3) Regarding ductility, beams with PVA fibers greatly enhance the ductility factor due to fulfilling microcracking and strain hardening behaviors. The ductility was improved by almost 52% and 20% for beams with PVA and hybrid fibers, respectively. GFRP bars reduced ductility by 19% by delaying the onset of yielding during loading.
4) Higher values of ultimate strain have appeared in beams with CA and hybrid fibers, which indicates the recording of a high level of warning before failure. Crack propagation is delayed by 38% and 63% with the inclusion of hybrid and CA fibers, respectively, indicating that short fibers limit the spread of cracking. Using GFRP instead

Table 8 Experimental and Nominal Flexural Strength

Author	Beam	fc' (Mpa)	Geometry		Bottom RFT		Fiber Parameters						M_{exp} (KN)	M_n (KN)	$\frac{Mexp}{Mn.}$
			b (mm)	t (mm)	HTS	GFRP	Vf1	(lf) (mm)	(ϕf) (mm)	Vf2	(lf) (mm)	(ϕf) (mm)			
Present	S1	44	120	250	*2Φ12+2Φ10*	–	–	–	–	–	–	–	65.80	59.71	1.10
	S2	50.3	120	250	*2Φ12+2Φ10*	–	–	–	–	1.2	10	0.01	100.0	101.06	0.99
	S3	44	120	250	–	*2G12+2G10*	–	–	–	–	–	–	121.0	117.25	1.03
	S4	48.4	120	250	–	*2G12+2G10*	0.6	8	0.015	0.6	10	0.01	143.2	157.50	0.91
	S5	46.5	120	250	–	*2G12+2G10*	1.2	8	0.015	–	–	–	128.9	132.07	0.98
	S6	50.3	120	250	–	*2G12+2G10*	–	–	–	1.2	10	0.01	160.9	168.93	0.95
	S7	50.3	120	250	*2Φ10*	*2G12*	–	–	–	1.2	10	0.01	137.0	136.76	1.00
Shanour et al. 2018	BF1	44	115	280	2Φ16	–	–	–	–	–	–	–	37.40	38.02	0.98
	BF2	44	115	280	2Φ16	–	1	12	0.04	–	–	–	44.9	45.08	1.00
	BF3	44	115	280	2Φ16	–	2	12	0.04	–	–	–	50.10	51.10	0.98
	BF4	44	115	280	2Φ16	–	0.5	12	0.04	0.5	12	0.02	41.3	47.66	0.87
	BF5	44	115	280	2Φ16	–	1	12	0.04	1	12	0.02	46.5	55.4	0.84
	BF6	44	115	280	2Φ16	–	2	12	0.04	–	–	–	46.8	49	0.96
	BF7	44	115	280	2Φ16	–	1	12	0.04	1	12	0.02	45.2	55.4	0.82
	BF8	44	115	280	2Φ12	–	–	–	–	–	–	–	26.3	22.1	1.19
	BF9	44	115	280	2Φ12	–	0.5	12	0.04	0.5	12	0.02	28.9	30.64	0.94
	BF10	44	115	280	2Φ12	–	1	12	0.04	1	12	0.02	32.8	38.74	0.85
	BF11	44	115	280	2Φ12	–	0.5	12	0.04	0.5	12	0.02	31.2	33.8	0.92
	BF12	44	115	280	2Φ12	–	1	12	0.04	1	12	0.02	35.4	42.62	0.83
Meng et al. 2017	SB1	45	100	200	2Φ12	–	–	–	–	–	–	–	16.25	15.22	1.0677
	SB2	47	100	200	2Φ12	–	2.2	12	0.04	–	–	–	21.4	20.46	1.0459
	SB3	49.8	100	200	2Φ12	–	–	–	–	–	–	–	16.25	15.33	1.06
	SB4	51.9	100	200	2Φ12	–	2.2	12	0.04	–	–	–	21.2	20.68	1.0251

Table 8 (continued)

Author	*Beam*	*fc'* *(Mpa)*	*Geometry*		*Bottom RFT*		*Fiber Parameters*						M_{exp} *(KN)*	*Mn* (KN)	$\frac{Mexp}{Mn.}$
			b (mm)	*t (mm)*	*HTS*	*GFRP*	*Vf1*	*(lf) (mm)*	*(ϕf) (mm)*	*Vf2*	*(lf) (mm)*	*(ϕf) (mm)*			
Ge et al. 2020	CBA	20	180	250	2Φ10	–	–	–	–	–	–	–	19.30	16.68	1.16
	EBA	31.4	150	200	2Φ12	–	2	12	0.04	–	–	–	22.5	22.16	1.02
	CBB	31.4	150	200	2Φ12	1G8	–	–	–	–	–	–	22	20.24	1.09
	EBB	31.4	150	200	2Φ12	1G8	2	12	0.04	–	–	–	24.8	26.56	0.93
	CBC	31.4	150	200	1Φ10	2G8	–	–	–	–	–	–	18.3	20.96	0.87
	EBC	31.4	150	200	1Φ10	2G8	2	12	0.04	–	–	–	21.9	27.16	0.81
	CBD	31.4	150	200	1Φ12	2G8	–	–	–	–	–	–	21.2	23	0.92
	EBD	31.4	150	200	1Φ12	2G8	2	12	0.04	–	–	–	27.1	29	0.93
	CBE	31.4	150	200	2Φ10	1G8	–	–	–	–	–	–	17.3	18.27	0.95
	EBE	31.4	150	200	2Φ10	1G8	2	12	0.04	–	–	–	19.7	24.88	0.79
	CBF	30.16	150	200	2Φ12	1G8	–	–	–	–	–	–	24.3	22.3	1.09
	EBF	31.4	150	200	2Φ12	1G8	2	12	0.04	–	–	–	26.8	28.4	0.94
	CBG	31.4	150	200	2Φ12	1G8	–	–	–	–	–	–	26.6	25.5	1.04
	EBG	31.4	150	200	2Φ12	1G8	2	12	0.04	–	–	–	27.2	31	0.88
Jie, et al. 2019	HB1	30	150	200	2Φ12	–	–	–	–	–	–	–	18.5	15	1.23
	HB2	31.4	150	200	2Φ12	–	2	12	0.04	–	–	–	19.5	19.46	1.0
	HB3	31.4	150	200	2Φ12	–	2	12	0.04	–	–	–	19.8	22.94	0.86
	HB4	31.4	150	200	2Φ12	–	2	12	0.04	–	–	–	22.5	24.12	0.93
	HC1	30	150	200	2Φ12	1G8	–	–	–	–	–	–	22	20.15	1.09
	HC2	31.4	150	200	2Φ12	1G8	2	12	0.04	–	–	–	23.9	24.1	0.99
	HC3	31.4	150	200	2Φ12	1G8	2	12	0.04	–	–	–	25.7	27.4	0.93
	HC4	31.4	150	200	2Φ12	1G8	2	12	0.04	–	–	–	25.4	28	0.90
Number of Speciems															45
Average															0.97
Standard Deviation															0.101
Coefficient of variation															10.4%

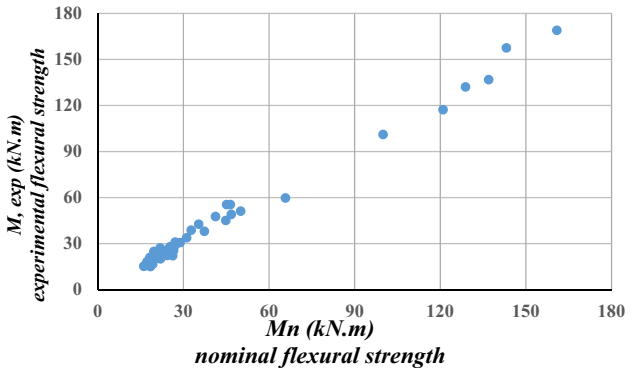

Fig. 22 Comparison between Experimental and Nominal Flexural Strength

of HTS bars accelerated crack formation in non-fibrous beams.

5) The results for toughness improvement indicate that both CA and hybrid fibers significantly increase toughness by 91% and 45% respectively, due to their high energy dissipation capacity during the cracking stage. Additionally, PVA fibers exhibit a 68% improvement in both tensile strength and elongation, attributable to their short fiber length. The test beams containing CA fibers show a roughly 30% increase in flexural strength relative to PVA fibers, as previously reported. Notably, GFRP bars decrease flexural toughness by 27% relative to HTS bars. However, GFRP bars indicate a 20% improvement in flexural strength against HTS bars when the reinforcement ratio is equal.
6) Using the NFEA applications for beams in this research revealed a strong correlation in both cracking patterns and load capacities. The mean ratio [Py, exp./Py, NA.] at the yield load stage was equal to 1.053, with a standard deviation of 0.118 and a coefficient of variation of 10.62%. Meanwhile, the mean ratio [Pu, exp./Pu, NA.] at the ultimate limit was 0.967, with a standard deviation of 0.06 and a coefficient of variation of 6.25%.
7) It concluded that the nominal flexural strength of HPRC beams, regardless of being reinforced with single or hybrid fibers, may be a valid predictor of flexural performance. An analytical analysis of 45 experimental tests of flexural performance from trials reported in the literature yields an average [M, exp.]./Mn.] of 0.97 overall average, with a standard deviation of 0.101 and a coefficient of variation of 10.4%.

Author Contributions Mahmoud Abbass: Writing—original draft, Investigation, Funding acquisition, Formal analysis, Data curation. Mohamed Said: Writing—review & editing, Validation, Supervision, Methodology, Investigation, Conceptualization. Ahmed Salah: Conceptualization, Investigation, Writing—review & editing. Maher Adam: Conceptualization, Supervision, Writing—review & editing.

Data Availability No datasets were generated or analysed during the current study.

Declarations

Conflict of interest The authors confirm that they have no financial conflicts of interest or personal relationships that could be perceived as influencing the work presented in this paper.

References

ACI Committee 544 (2018) ACI PRC-544.4-18: Guide to Design with Fiber-Reinforced Concrete. American Concrete Institute, Farmington Hills, MI
ACI 318–19 (2019) Building code requirements for structural concrete. American Concrete Institute
ACI Committee 544 (2023) ACI PRC-544.1R-96: Report on Fiber Reinforced Concrete (Reapproved 2023). American Concrete Institute, Farmington Hills, MI
Adam MA, Said M, Mahmoud AA, Shanour AS (2015) Analytical and experimental flexural behavior of concrete beams reinforced with glass fiber reinforced polymers bars. Constr Build Mater 84:354–366
ANSYS (2009) A Finite Element Computer Software and User Manual for Nonlinear Structural Analysis, Release Version 12.1.0. ANSYS Inc, Canonsburg, PA
Asok G, George S (2016) Investigation on hybrid concrete using steel and polypropylene fiber. Int J New Technol Res 2(5)
Charron J-P, Desmettre C, Androuët C (2020) Flexural and shear behaviors of steel and synthetic fiber reinforced concretes under quasi-static and pseudodynamic loadings. Constr Build Mater 238:117659. https://doi.org/10.1016/j.conbuildmat.2019.117659
Dong H-L, Zhou W, Wang Z (2019) Flexural performance of concrete beams reinforced with FRP bars grouted in corrugated sleeves. Compos Struct 215:49–59
Douglas D (2012) An Investigation into the Flexural Behavior of GFRP Reinforced Concrete Beams, [MSc thesis], University of Toronto, Canada
Gao J, Sha A, Wang Z, Hu L, Yun D, Liu Z et al (2018) Characterization of carbon fiber distribution in cement-based composites by computed tomography. Construct Build Mater 177:134–147
Ge W-J, Ashour AF, Yu J, Gao P, Cao D-F, Cai C, Ji X (2019) Flexural behavior of ECC–concrete hybrid composite beams reinforced with FRP and steel bars. J Compos Constr 23(1):04018069. https://doi.org/10.1061/(ASCE)
Ge W, Song W, Ashour AF, Lu W, Cao D (2020) Flexural performance of FRP/steel hybrid reinforced engineered cementitious composite beams. J Building Eng 31. https://doi.org/10.1016/j.jobe.2020.101329
Guo Z, Zhuang C, Li Z, Chen Y (2021) Mechanical properties of carbon fiber reinforced concrete (CFRC) after exposure to high temperatures. Compos Struct 256:113072. https://doi.org/10.1016/j.compstruct.2020.113072
Habeeb MN, Ashour AF (2008) Flexural behavior of continuous GFRP reinforced concrete beams. J Compos Constr 12(2):115–124
Hieu NT, Tuan Nvan (2021) Effect of loading rate on flexural behavior of concrete and reinforced concrete beams. J Sci Technol Civil Eng (STCE) - NUCE 15(3):136–143. https://doi.org/10.31814/stce.nuce2021-15(3)-11
Joyklad P, Krishna Gadagamma C, Maneengamlert B, Nawaz A, Ejaz A, Hussain Q, Saingam P (2024) Structural behavior of RC one-way

slabs strengthened with ferrocement and FRP composites. Eng Fail Anal 161. https://doi.org/10.1016/j.engfailanal.2024.108328
Li B, Chi Y, Xu L, Shi Y, Li C (2018) Experimental investigation on the flexural behavior of steel-polypropylene hybrid fiber reinforced concrete, Constr. Build. Mater. 191 80–94. https://doi.org/10.1016/j.conbuildmat.2018.09.202
Liew KM, Akbar A (2020) The recent progress of recycled steel fiber reinforced concrete. Constr Build Mater 232:117232. https://doi.org/10.1016/j.conbuildmat.2019.117232
Liu F, Ding W, Qiao Y (2020) Experimental investigation on the tensile behavior of hybrid steel-PVA fiber reinforced concrete containing fly ash and slag powder. Constr Build Mater 241:118000. https://doi.org/10.1016/j.conbuildmat.2020.118000
Meng D, Lee CK, Zhang YX Flexural and shear behaviours of plain and reinforced polyvinyl alcohol-engineered cementitious composite beams. Eng Struct (2017), 151, 261–272. https://doi.org/10.1016/j.engstruct.2017.08.036
Pakravan HR, Latifi M, Jamshidi M (2016) Ductility improvement of cementitious composites reinforced with polyvinyl alcohol-polypropylene hybrid fibers, J Ind, Text;45(5)
Pawłowski D, Szumigała M (2015) Flexural behaviour of full-scale basalt FRP RC beams – experimental and numerical studies. Procedia Eng 108:518–525. https://doi.org/10.1016/j.proeng.2015.06.114
Pawłowski D, Szumigała M (2015) Flexural behavior of full-scale basalt FRP RC beams experimental and numerical studies. Procedia Eng 108:518–525
Pecce M, Manfredi G, Cosenza E (2000) Experimental response and code models of GFRP RC beams in bending. J Compos Constr 4(4):182–190
Rafid S (2019) A case study on concrete column strength improvement with different steel fibers and polypropylene fibers. J Mater Res Technol 8:6106–6114
Raffaello F, Andrea P, Domenico (2007) A Limit States Design of Concrete Structures Reinforced with FRP Bars, [Ph.D. thesis], Italy, University of Naples Federico
Rodsin K, Ejaz A, Hussain Q, Parichatprecha R (2023) Experimental and Analytical Studies on Low-Cost Glass-Fiber-Reinforced-Polymer-Composite-Strengthened Reinforced Concrete Beams: A Comparison with Carbon/Sisal Fiber-Reinforced Polymers. Polymers 15(19). https://doi.org/10.3390/polym15194027
Romualdi JP, Mandel JA (1964) Tensile strength of concrete affected by uniformly distributed closely spaced short lengths of wire reinforcement. ACI J 61:657–671
Romualdi NP, Batson GB (1963) Mechanics of crack arrest in concrete. ASCE Eng Mech 89:147–168
Said M, Adam MA, Mahmoud AA, Shanour AS (2016) Experimental and analytical shear evaluation of concrete beams reinforced with glass fiber reinforced polymers bars. Constr Build Mater 102:574–591
Said M, Salah A, Erfan A, Esam A (2023) Experimental analysis of torsional behavior of hybrid fiber reinforced concrete beams. J Building Eng 71. https://doi.org/10.1016/j.jobe.2023.106574
Saingam P, Chatveera B, Roopchalaem J, Hussain Q, Ejaz A, Khaliq W, Makul N, Chaimahawan P, Sua-iam G (2025) Influence of recycled electronic waste fiber on the mechanical and durability characteristics of eco-friendly self-consolidating mortar incorporating recycled glass aggregate. Case Stud Constr Mater 22. https://doi.org/10.1016/j.cscm.2025.e04369
Shanour AS, Said M, Arafa AI, Maher A (2018) Flexural performance of concrete beams containing engineered cementitious composites. Constr Build Mater 180:2334
Smarzewski P (2018) Hybrid fibres as shear reinforcement in high-performance concrete beams with and without openings. Appl Sci 8. https://doi.org/10.3390/app8112070
Soric Z, Kisicek T, Galic J (2010) Deflections of concrete beams reinforced with FRP bars. Mater Struct 43(S1):73–90
Suparp S, Khan I, Ejaz A, Khan K, Weesakul U, Hussain Q, Saingam P (2023) Behavior of non-prismatic RC beams with conventional steel and green GFRP rebars for sustainable infrastructure. Sci Rep 13(1). https://doi.org/10.1038/s41598-023-41467-w
Tomlinson D, Fam A (2015) Performance of concrete beams reinforced with basalt FRP for flexure and shear. J Compos Constr 19(2):04014036.
Tu Y, Zhang J, Qian Y (2009) Experimental and theoretical investigation of flexural load carrying capacity of concrete beams reinforced with AFRP tendons. J Southeast Univ (Nat Sci) China 39(3):563–568
Wang Z, Ma G, Ma Z, Zhang Y (2021) Flexural behavior of carbon fiber-reinforced concrete beams under impact loading. Cem Concr Compos 118:103910. https://doi.org/10.1016/j.cemconcomp.2020.103910
Wang Z, Ma G, Ma Z, Zhang Y (2021) Flexural behavior of carbon fiber-reinforced concrete beams under impact loading. Cem Concr Compos 118. https://doi.org/10.1016/j.cemconcomp.2020.103910
Wei ZW, Wang TS, Li HJ, Dong TC, Li Z, Guo X Study of the flexural behavior of basalt fiber-reinforced concrete beams with basalt fiber-reinforced polymer bars and steel bars. Case Stud Constr Mater, 22. https://doi.org/10.1016/j.cscm.2025.e04433
Wei B, He X, Zhang S, Tang Z, Wang H, Zhou M (2025) Experimental study on mechanical properties of hybrid fiber-reinforced high-strength concrete and flexural toughness of beams. J Building Eng. https://doi.org/10.1016/j.jobe.2025.113905
Yooprasertchai E, Khursheed A, Qureshi MI, Ejaz A, Hussain Q, Jirasakjamroonsri A, Saingam P (2024) Sustainable development of concrete through treated and untreated plastic waste aggregates. Sci Rep 14(1). https://doi.org/10.1038/s41598-024-73236-8